

Comparative theoretical analysis between parallel and perpendicular geometries for 2D particle patterning in photovoltaic ferroelectric substrates

C. Arregui

Dep. Mecánica de Fluidos y Propulsión Aeroespacial, Universidad Politécnica de Madrid, Plaza del Cardenal Cisneros 3, 28040 Madrid, Spain

J. B. Ramiro
j.ramiro@upm.es

Dep. Mecánica de Fluidos y Propulsión Aeroespacial, Universidad Politécnica de Madrid, Plaza del Cardenal Cisneros 3, 28040 Madrid, Spain

A. Alcázar

Dep. Mecánica de Fluidos y Propulsión Aeroespacial, Universidad Politécnica de Madrid, Plaza del Cardenal Cisneros 3, 28040 Madrid, Spain

A. Méndez

Dep. Mecánica de Fluidos y Propulsión Aeroespacial, Universidad Politécnica de Madrid, Plaza del Cardenal Cisneros 3, 28040 Madrid, Spain

J. F. Muñoz-Martínez

Dep. Mecánica de Fluidos y Propulsión Aeroespacial, Universidad Politécnica de Madrid, Plaza del Cardenal Cisneros 3, 28040 Madrid, Spain

M. Carrascosa

Dep. Física de Materiales, Universidad Autónoma de Madrid, Cantoblanco, 28049 Madrid, Spain

This paper describes the dielectrophoretic potential created by the evanescent electric field acting on a particle near a photovoltaic crystal surface depending on the crystal cut. This electric field is obtained from the steady state solution of the Kukhtarev equations for the photovoltaic effect, where the diffusion term has been disregarded. First, the space charge field generated by a small, square, light spot where $d \ll l$ (being d a side of the square and l the crystal thickness) is studied. The surface charge density generated in both geometries is calculated and compared as their relation determines the different properties of the dielectrophoretic potential for both cuts. The shape of the dielectrophoretic potential is obtained and compared for several distances to the sample. Afterwards other light patterns are studied by the superposition of square spots, and the resulting trapping profiles are analysed. Finally the surface charge densities and trapping profiles for different d/l relations are studied.

[DOI: <http://dx.doi.org/10.2971/jeos.2015.15026>]

Keywords: Optoelectronic tweezers, photovoltaic tweezers, particle trapping, dielectrophoresis, nanoparticles

1 INTRODUCTION

Recently, techniques for trapping and manipulation of particles with size as small as possible have become an important research field. Several strategies have been proposed and developed that rely on optical [1, 2], electrokinetic [3, 4] and pyroelectric [5, 6] effects. One of these techniques, the so-called photovoltaic tweezers, recently proposed, is based in the bulk photovoltaic (PV) effect of certain ferroelectric materials [7] and is becoming important for its capacity to manipulate many particles in parallel using low-intensity light patterns [8]. These techniques make use of the evanescent electric fields generated by the PV effect on the surface of certain ferroelectric materials [9]–[12]. This effect makes it possible to manipulate particles via electrophoretic (EP) or dielectrophoretic (DEP) forces, for charged and uncharged particles, respectively. In particular, lithium niobate (LN) is a reference photovoltaic material whose capabilities to trap and manipulate particles, have been thoroughly studied [4, 12] and it is being used in many experiments [13]–[18]. It is well known that optical anisotropy of ferroelectric materials makes them to behave differently depending on the direction on their C-axis. But there is no work studying the dependence of the particle-trapping features on the crystal cut. However, in or-

der to take full advantage of these capabilities, such analysis becomes necessary to choose the best crystal geometry for each purpose.

This paper aims to describe the evanescent electric field that acts on a particle near a PV crystal surface depending on the crystal cut. Light interaction with photovoltaic materials is a complex process and each cut has its own particularities. So, it is not possible to undertake an in-depth study of the evanescent electric field generated by a light pattern without accounting for details such as the concrete light pattern or the impurity concentration of the material, which implies a lack of generality and makes it difficult to draw conclusions. This paper aims to describe how the crystal cut affects particle trapping and to offer a general outlook to help the researcher choose the best configuration for a particular purpose. To make the description valid for as many situations as possible, we will start from a steady state solution of the Kukhtarev equations for the photorefractive effect [19, 20]. Next, we disregard diffusion term as it is much smaller than the photovoltaic term. Also, it has no preferred direction, so its effect does not depend on the crystal cut. The obtained space-charge field gives rise to the evanescent electric field, but the movement of the

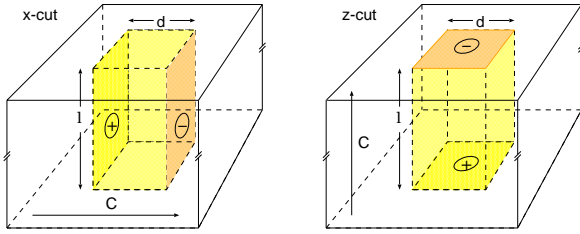


FIG. 1 Charge distribution due to a square light pattern for X-cut and Z-cut geometries.

particles under this field is not straight forward. To give the reader a clear idea of the particle trapping, in this paper we will show the attractive potential the particles experience due to this electric field. We call it DEP Potential (V_{DEP}).

For the sake of simplicity, a small homogeneously illuminated square is considered in both geometries, with a size much smaller than the sample thickness. This geometry has been chosen to compare with the resolution of the spatial light modulators (SLM) -from now on a pixel, considering that these devices are used in many particle trapping experiments [11, 13, 21]. More complicated patterns could be generated using a pattern of such small pixels as it is shown in Section 3.2. Also, different ratios between pixel size and crystal thickness are analyzed in Section 3.3.

2 THEORETICAL MODEL

2.1 Bulk and evanescent space charge field

The main purpose of this work is to analyze the DEP trapping generated by a particular light pattern, depending on the crystal orientation. In order to obtain a qualitative description of the space charge field generated in the crystal, we will simplify as much as possible the physical processes involved in the charge distribution inside the material under illumination. This can be done just by analyzing the current density from the Kukhtarev equations, \vec{J} , disregarding the diffusion term, much smaller than the photovoltaic one [22]. That is:

$$\vec{J} = q\mu n\vec{E} + qsIN_D L_{PV} \vec{u}_{PV} \quad (1)$$

where N_D is the donor concentration, s the photo-ionization cross section, I the light intensity, μ the mobility, \vec{E} the total electric field, L_{PV} the photovoltaic transport length and \vec{u}_{PV} the unit vector in the direction of the polar axis. Note that, in the steady state, provided an open circuit situation, $\vec{J} = 0$, and

$$\vec{E} = -\frac{sIN_D L_{PV}}{\mu n} \vec{u}_{PV} \quad (2)$$

in saturable media $\vec{E} = \vec{E}_{sat} \neq \vec{E}(I)$ (note that, in the above expression, $n \propto I$). Therefore, within this approach, when the crystal is illuminated with an homogeneous square light pattern, the charges will distribute homogeneously on the walls of an illuminated cuboid, in the direction of the polar axis as it is shown in Figure 1. Consequently, for an homogeneously illuminated spot on the surface of the crystal, the charge will be distributed in two planes. This planes are perpendicular to the surface for X- or Y-cut configuration and contained on the surface for Z-cut. This difference between both distributions results in very distinct DEP forces. As X-cut and Y-cut are equivalent for our purposes, from now on X-cut geometry will be used to represent both of them.

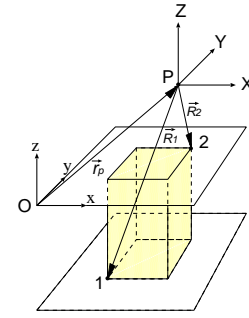


FIG. 2 Coordinate system for each point (P) outside the crystal. Points (1) and (2) are opposite corners of the illuminated cuboid.

The evanescent field produced by the internal electric field modifies the electronic cloud of the particles in the surroundings of the crystal and moves them accordingly. The interaction can be described in terms of the multipolar expansion of the particle: charge, dipole, quadrupole, and higher-order multipoles. For electrically neutral particles, with no permanent multipoles, the strongest interaction with the spacecharge field of the crystal comes from the induced dipole. In this work, we will assume that particles are electrically neutral, isotropic and small compared with the illuminated region, so the dipole approximation can be safely applied [23, 24].

This leads to an DEP force given by:

$$\vec{F} = \vec{\nabla} \left(-\vec{p} \cdot \vec{E} \right) = \vec{\nabla} \left(-\epsilon_0 \alpha E^2 \right) \quad (3)$$

where \vec{p} is the induced dipolar moment and α is the scalar particle polarizability. [8, 9, 25]. As DEP force is equal to the gradient of a spatial function, a DEP potential, V_{DEP} , independent of the particle polarizability α , can be defined:

$$V_{DEP} = -\epsilon_0 E^2 \quad (4)$$

Once the electric field is known, V_{DEP} is easily obtained from Eq. (4).

2.2 Electric field outside the crystal

To fulfill the conditions of section 2.1, the illuminated area (d^2) of the crystal is assumed to be square and very small compared to the thickness (l) of the crystal, so that $d \ll l$ (where $d = x_2 - x_1 = y_2 - y_1$ and $l = z_2 - z_1$, see Figure 2). In the present approximation the charge is homogeneously distributed at opposite faces across the C-axis in the light cuboid (top and bottom for Z-cut and vertical walls for X-cut), acting like a finite-area plane capacitor. To obtain the electric field outside the cuboid at point P , let $\vec{r}_p = (x_p; y_p; z_p)$ be the position vector of point P in a reference system (Oxyz) stuck to the crystal, in which the edges of the cuboid have coordinates $x_1; x_2; y_1; y_2; z_1; z_2$. Let's define another coordinate system PXYZ parallel to Oxyz and centered at P . The cuboid vertices in PXYZ are:

$$X_i = x_i - x_p$$

$$Y_i = y_i - y_p$$

$$Z_i = z_i - z_p$$

and the distance from P to each vertex is $R_{ijk} = \sqrt{X_i^2 + Y_j^2 + Z_k^2}$ where $i; j; k = \{1; 2\}$. The evanescent electric field \vec{E}^P at point P writes: where σ_x and σ_z are the

2.2.1 X-cut

$$\begin{aligned} \vec{E}_x^P &= \frac{\sigma_x}{4\pi\epsilon_0\epsilon_r} \left[\arctan\left(\frac{Z_2 Y_2}{X_2 R_{222}}\right) - \arctan\left(\frac{Z_2 Y_1}{X_2 R_{212}}\right) - \arctan\left(\frac{Z_1 Y_2}{X_2 R_{221}}\right) + \arctan\left(\frac{Z_1 Y_1}{X_2 R_{211}}\right) \right. \\ &\quad \left. - \arctan\left(\frac{Z_2 Y_2}{X_1 R_{122}}\right) + \arctan\left(\frac{Z_2 Y_1}{X_1 R_{112}}\right) + \arctan\left(\frac{Z_1 Y_2}{X_1 R_{121}}\right) - \arctan\left(\frac{Z_1 Y_1}{X_1 R_{111}}\right) \right] \\ \vec{E}_y^P &= \frac{\sigma_x}{4\pi\epsilon_0\epsilon_r} \log\left(\frac{(Z_2 + R_{212})(Z_1 + R_{221})(Z_1 + R_{111})(Z_2 + R_{122})}{(Z_1 + R_{211})(Z_2 + R_{222})(Z_2 + R_{112})(Z_1 + R_{121})}\right) \\ \vec{E}_z^P &= \frac{\sigma_x}{4\pi\epsilon_0\epsilon_r} \log\left(\frac{(Y_2 + R_{221})(Y_1 + R_{212})(Y_1 + R_{111})(Y_2 + R_{122})}{(Y_1 + R_{211})(Y_2 + R_{222})(Y_2 + R_{121})(Y_1 + R_{112})}\right) \end{aligned} \quad (5)$$

2.2.2 Z-cut

$$\begin{aligned} \vec{E}_x &= \frac{\sigma_z}{4\pi\epsilon_0\epsilon_r} \log\left(\frac{(Y_2 + R_{122})(Y_1 + R_{212})(Y_1 + R_{111})(Y_2 + R_{221})}{(Y_1 + R_{112})(Y_2 + R_{222})(Y_2 + R_{121})(Y_1 + R_{211})}\right) \\ \vec{E}_y &= \frac{\sigma_z}{4\pi\epsilon_0\epsilon_r} \log\left(\frac{(X_2 + R_{212})(X_1 + R_{122})(X_1 + R_{111})(X_2 + R_{221})}{(X_1 + R_{112})(X_2 + R_{222})(X_2 + R_{211})(X_1 + R_{121})}\right) \\ \vec{E}_z^P &= \frac{\sigma_z}{4\pi\epsilon_0\epsilon_r} \left[\arctan\left(\frac{X_2 Y_2}{Z_2 R_{222}}\right) - \arctan\left(\frac{X_2 Y_1}{Z_2 R_{212}}\right) - \arctan\left(\frac{X_1 Y_2}{Z_2 R_{122}}\right) + \arctan\left(\frac{X_1 Y_1}{Z_2 R_{112}}\right) \right. \\ &\quad \left. - \arctan\left(\frac{X_2 Y_2}{Z_1 R_{221}}\right) + \arctan\left(\frac{X_2 Y_1}{Z_1 R_{211}}\right) + \arctan\left(\frac{X_1 Y_2}{Z_1 R_{121}}\right) - \arctan\left(\frac{X_1 Y_1}{Z_1 R_{111}}\right) \right] \end{aligned} \quad (6)$$

surface charge densities for the X- and Z-cut, respectively

2.3 Surface charge density

To compare the evanescent fields for X- and Z-cuts, it is necessary to obtain the σ_x/σ_z ratio. This relation can be determined taking into account that the steady-state electric field inside the light cuboid, E_{sat} , only depends on photovoltaic length, not on C-axis orientation. Therefore, this field, given by Eq. (2), has the same module for both cuts and is proportional to the surface charge density. In addition, as we have assumed negligible diffusion transport, the bulk electric field is parallel to the polar axis and so the x-component of the electric field for the X-cut sample equals the z-component of it for the Z-cut sample. Applying the same reasoning, in the center of the cuboid, where no edge effect is expected and no other component of the electric field but the above-mentioned appears, both fields are equal in module:

$$E_{sat} = E_x^{X-cut} = E_z^{Z-cut} \quad (7)$$

As in the center of the cuboid $X_1 = Y_1 = -d/2$, $X_2 = Y_2 = d/2$, $Z_1 = -l/2$, $Z_2 = l/2$, Eqs. (5) and (6) simplify. In this case the electric field for a finite-area plane capacitor writes:

$$E_x^{X-cut} = \frac{2\sigma_x}{\pi\epsilon_0\epsilon_r} \arctan\left(\frac{l/d}{\sqrt{2+(l/d)^2}}\right) \quad (8)$$

$$E_y^{X-cut} = E_z^{X-cut} = 0 \quad (9)$$

$$E_y^{Z-cut} = E_x^{Z-cut} = 0 \quad (10)$$

$$E_z^{Z-cut} = \frac{2\sigma_z}{\pi\epsilon_0\epsilon_r} \arctan\left(\frac{1}{(l/d)\sqrt{2+(l/d)^2}}\right) \quad (11)$$

From the expressions above, one can obtain the surface charge densities

$$\frac{\sigma_x}{\pi\epsilon_0\epsilon_r E_{sat}/2} = \frac{1}{\arctan\left(\frac{l/d}{\sqrt{2+(l/d)^2}}\right)} \quad (12)$$

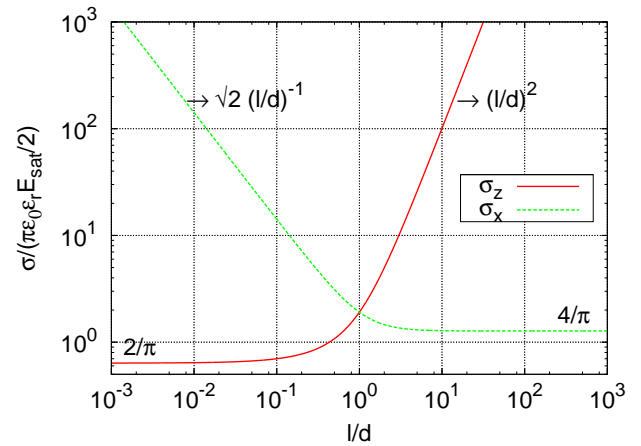


FIG. 3 Logarithmic plots of the dimensionless surface charge densities for Z-cut and X-cut as functions of l/d . Asymptotic values and tendency for the limits $l/d \rightarrow 0$ and $l/d \rightarrow \infty$ are also shown.

$$\frac{\sigma_z}{\pi\epsilon_0\epsilon_r E_{sat}/2} = \frac{1}{\arctan\left(\frac{1}{(l/d)\sqrt{2+(l/d)^2}}\right)} \quad (13)$$

The evolution of the dimensionless surface charge density $\sigma_z^* = \sigma_z/(\pi\epsilon_0\epsilon_r E_{sat}/2)$ and $\sigma_x^* = \sigma_x/(\pi\epsilon_0\epsilon_r E_{sat}/2)$ with l/d is shown on the logarithmic plot of Figure 3. σ_z grows like $(l/d)^2$ for $l/d \gtrsim 1$ whereas σ_x remains constant in this region $\sigma_x^* \rightarrow 4/\pi$. On the other hand, for $l/d \lesssim 1$, the values for σ_z tends to a constant ($\sigma_z^* \rightarrow 2/\pi$), and σ_x behaves as $(l/d)^{-1}$. This figure shows the dependence of the surface charge density created by a square illumination spot on the size of this spot (assuming that l is constant and d varies). Each geometry shows two different regimes that must be considered in order to estimate the trapping capability of an illumination pattern. This dependence will be used later in this work to study the dependence of V_{DEP} with l/d .

To study the relation between V_{DEP} values of X- and Z-cut crystals it is necessary to calculate the ratio between the sur-

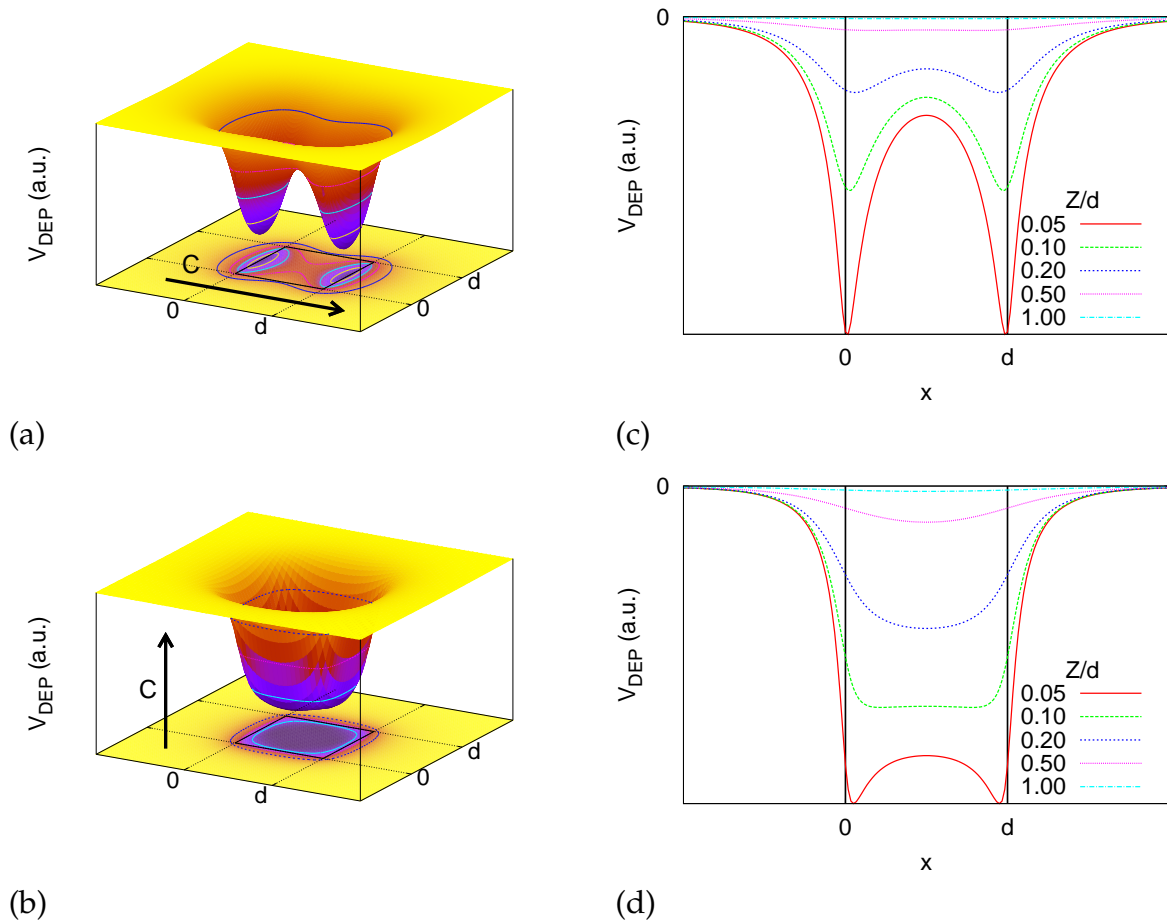


FIG. 4 3D plot of the V_{DEP} for a dimensionless distance to the surface $z/d = 0.1$ in (a) X-cut and (b) Z-cut. V_{DEP} curves along the x-axis for different z/d values in (c) X-cut and (d) Z-cut.

face charge densities for both geometries, which is:

$$\frac{\sigma_z}{\sigma_x} = \frac{\arctan \frac{l/d}{\sqrt{2+(l/d)^2}}}{\arctan \frac{1}{(l/d)\sqrt{2+(l/d)^2}}} \quad (14)$$

When $l/d \gg 1$ the numerator of the previous equation tends to $\arctan(d/l) \sim \pi/4$ (since $d/l \ll 1$ and for small arguments $\arctan(\epsilon) \approx \epsilon$) and the denominator tends to $(l/d)^2$ so

$$\lim_{l/d \rightarrow \infty} \left(\frac{\sigma_z}{\sigma_x} \right) = \frac{\pi}{4} \left(\frac{l}{d} \right)^2 \quad (15)$$

$$\lim_{l/d \rightarrow 0} \left(\frac{\sigma_z}{\sigma_x} \right) = \frac{\sqrt{2}}{\pi} \left(\frac{l}{d} \right) \quad (16)$$

In order to give numerical values in the next section we use $\sigma_x = 1$ and $l/d = 1000$, so $\sigma_z/\sigma_x \sim 8 \cdot 10^5$ (these values are given only as a reference). σ_x depends on the PV field of the material and σ_z/σ_x on l/d .

3 RESULTS

3.1 Electric field generated by a single pixel

The evanescent electric field outside the crystal, near the illumination pattern can be calculated using Eqs. (5) and (6), and V_{DEP} can be obtained using Eq. (4). The results of these calculations for X- and Z- cut are shown in Figure 4(a) and 4(b), respectively.

In Z-cut samples, (Figure 4(b) and 4(d)), all the illuminated area has a significant value of V_{DEP} , which increases as we approach the material until we reach a plateau. If we continue approaching some edge effects appear, though only for positions very close to the crystal ($Z/d \leq 0.05$). For example, for an illuminated spot of 1 square micron, edge effects will appear at a distance $Z = 50$ nm and they will only affect particles with a size in the order or smaller than this distance. In X-cut samples the potential shows two peaks above each charged side of the light cuboid and decreases almost with the same slope at both sides of it (Figure 4(a) and 4(c)). If we study the potential as a function of the distance (Figure 4(c) and 4(d)) it can be seen that V_{DEP} decreases at a similar rate for both orientations. Finally, due to the big difference in the values of σ , the potential well is much deeper in Z-cut samples for the same illumination intensity.

Therefore, the potential generated by an X-cut crystal has significant values only at the edges of the illuminated zone while Z-cut crystals can trap particles over all the illuminated area. This fact generates very different trapping patterns depending on the orientation of the crystal. The main differences between both orientations are:

- Z-cut crystal accurately traps particles along the illuminated region, but it is important to notice the possible appearance of edge effects, as can be observed in the shortest distance in Figure 4(b).

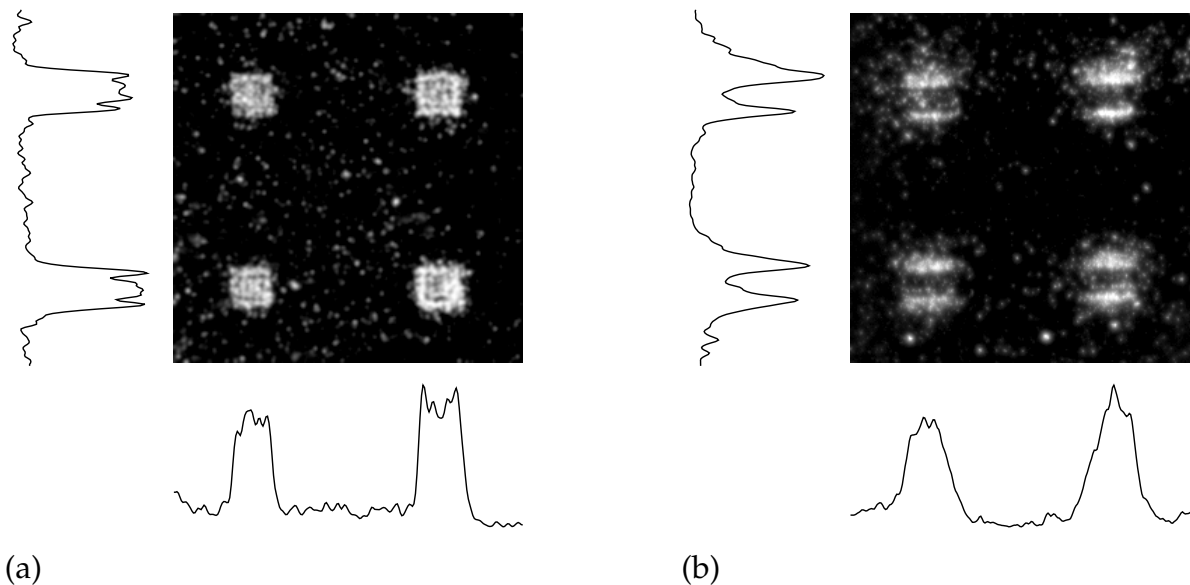


FIG. 5 Photograph and particle concentration profiles of the experimental pattern of aluminum nanoparticles trapped over a Fe:LiNbO₃ crystal previously exposed to a light pattern of 2x2 squares of 240 μm side. (a) Z-cut geometry, (b) X-cut geometry.

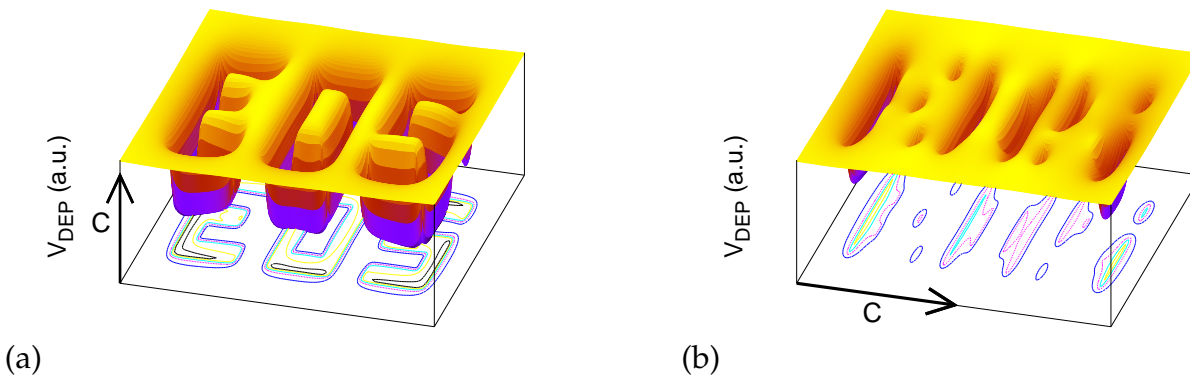


FIG. 6 X- (a) and Z-cut (b) V_{DEP} at a distance to the surface of $z/d = 0.1$. The [animation](#) shows the evolution of V_{DEP} from $z/d = 2$ to $z/d = 0$ for both cuts.

- In Z-cut crystal trapping pattern is analogous to the light pattern.
- In X-cut crystal trapping only occurs along the direction perpendicular to the Z-axis providing thin trapping zones normal to the polar axis.
- The V_{DEP} minimum is much deeper in Z-cut samples.

In order to compare the theoretical predictions with experiment we have carried out two simple experiments of particle trapping using the two crystal geometries. In this experiment a X-cut and a Z-cut samples of 1 mm thick Fe:LiNbO₃ crystal highly doped with iron (0.1% wt) have been illuminated by a cw doubled Nd:YAG laser ($\lambda = 532$ nm). A light pattern (consisting in a matrix of square light spots of 240 μm side, separated by 1 mm) is projected onto the sample using a spatial light modulator (Holoeye LC R1080 model). The intensity of the light that reaches the sample is 500 mW/cm² and it is maintained for 10 minutes. After substrate illumination, neutral aluminium nanoparticles (diameter ~ 70 nm) were deposited from a non-polar hexane suspension in which the substrate is immersed for 30 s (aluminium concentration 0.1 g/l). The obtained particle patterns do not depend on the specific sur-

face (+Z or -Z) illuminated, as expected from dielectrophoretic trapping of neutral particles. Figure 5 show clear differences on the trapping patterns corresponding to each crystal geometry that are in good agreement with the theoretical V_{DEP} shown in Figure 4.

3.2 Electric field generated by light patterns

Once the features of a single pixel have been analyzed it is possible to predict the trapping pattern of a specific light pattern like the one generated by a phase modulator, since it consists of a set of light pixels. We consider that the shape resulting by joining several pixels maintains the ratio of $d/l \ll 1$. We have applied this simple method to simulate the example of a two dimensional pattern using both X- and Z-cut geometries. The results are shown in Figure 6 which includes an animation. Both, figure and [animation](#), shows the different V_{DEP} created by a crystal illuminated with the acronym "EOS" for X- and Z-cut, for a particular distance of $z/d = 0.1$ (in the figure) and for different distances to the sample (in the animation). It can be observed that the trapping zone (that with low values of the V_{DEP}) is much larger in Z-cut crystals where, also, the po-

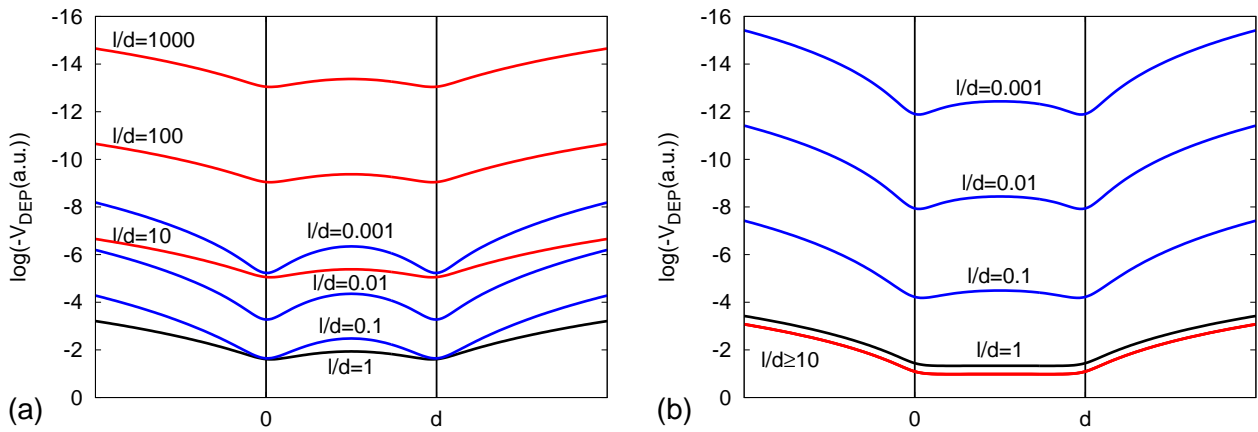


FIG. 7 V_{DEP} for different l/d ratios at a distance of $Z/d = 0.1$ in (a) X-cut and (b) Z-cut

tential reproduces with fidelity the light pattern in the near proximity of the crystal.

3.3 Different l/d ratios

Finally, although it is not the main purpose of this work, it can be interesting to analyze the qualitative results for different l/d ratios. The present study is valid for $l/d \gg 1$ but, even if this condition is not fulfilled, this analysis can also be useful taking into account some considerations.

When $l \approx d$ (nearly a cube) $\sigma_z/\sigma_x \approx 1$ so V_{DEP} for a given distance will be similar for both geometries, and, therefore, the distance between opposed charged faces are now in the order of the face size. If we continue increasing the illuminated spot, d becomes larger than l (i.e. a 1 cm² spot in a 1 mm depth crystal). So, in Z-cut samples, opposite charged faces are very near compared with d and its interaction becomes important. On the other hand, in X-cut samples, charged faces are far away and do not interact between them, also the proportion of charges near the surface is bigger than in Z-cut crystals.

Figure 7 shows V_{DEP} for several l/d ratios for X- (Figure 7(a)) and Z-cut (Figure 7(b)) where the value of l remains constant and d varies (i.e. the thickness of the crystal is the same and the illumination spot varies). Although the units of the ordinates axis are arbitrary, they are the same in both graphs so they can be compared. Both cuts present a minimum value near $l/d = 1$ but, while in Z-cut crystals this value remains almost constant when $l > d$, in X-cut samples it increases abruptly. When $l < d$ the value of the potential decreases with l in both cuts but it is more pronounced in Z-cut. Finally, in Z-cut crystals, the shape of the potential is almost independent of l/d . Only the center of the spot presents a minimum, more pronounced as l/d becomes smaller. In X-cut crystals, the bigger the distance between the charged faces, the steeper V_{DEP} decays at the middle of both faces. Note that when l/d is small, as l remains constant, d is large.

4 CONCLUSIONS

A simple model that includes all the relevant mechanisms for a qualitative and semi-quantitative study of the external elec-

tric field generated by an homogeneously illuminated cuboid in a photovoltaic crystal has been developed. It has been applied to study the differences in the DEP trapping capabilities of the two possible crystal geometries -parallel and perpendicular. A DEP potential (V_{DEP}) has been defined and obtained by an analytic expression for the electric field generated by the charge distribution of the crystal, comparing the surface density charge of geometries parallel and perpendicular to the polar axis. It has been observed that Z-cut V_{DEP} has a better spatial resolution and higher fidelity to reproduce (as trapping) the illumination pattern than X-cut. However, in Z-cut samples the existence of edge effects seem to make this cut more sensitive to the size of the illuminated area. On the other side X-cut crystals allows more defined trapping zones on the sides of the illuminated areas. This model has been extended to a more complex pattern where additional cooperative effects appear on the edges of the whole pattern.

Finally, it has been observed that the surface charge density strongly depends on the crystal geometry and on the l/d ratio. As V_{DEP} depends quadratically on σ , the estimation of its value is very important to know *a priori* which cut will have a bigger V_{DEP} well.

5 ACKNOWLEDGMENTS

This work was supported by the Spanish Ministerio de Economía y Competitividad under grants MAT2011-28379-C03 and MAT2014-57704-C3

References

- [1] A. Ashkin, "Acceleration and Trapping of Particles by Radiation Pressure," Phys. Rev. Lett. **24**, 156-159 (1970).
- [2] D. G. Grier, "A revolution in optical manipulation," Nature **424**, 810-816 (2003).
- [3] M. C. Wu, "Optoelectronic tweezers," Nat. Photonics **5**, 322-324 (2011).
- [4] A. Jonás and P. Zemánek, "Light at work: The use of optical forces for particle manipulation, sorting, and analysis," Electrophoresis. **29**, 4813-4851 (2008).

- [5] F. Laurell, M. G. Roelofs, W. Bindloss, H. Hsiung, A. Suna, and J. D. Bierlein, "Detection of ferroelectric domain reversal in KTiOPO_4 waveguides," *J. Appl. Phys.* **71**, (1992).
- [6] S. Grilli and P. Ferraro, "Dielectrophoretic trapping of suspended particles by selective pyroelectric effect in lithium niobate crystals," *Appl. Phys. Lett.* **92**, 232902-232902-3 (2008).
- [7] B. I. Sturman and V. M. Fridkin, *The photovoltaic and photorefractive effects in noncentrosymmetric materials* (Gordon and Breach Science Publishers, Philadelphia, 1992).
- [8] J. Villarroel, H. Burgos, Á. García-Cabañes, M. Carrascosa, A. Blázquez-Castro, and F. Agulló-López, "Photovoltaic versus optical tweezers," *Opt. Express* **19**, 24320-24330 (2011).
- [9] H. A. Eggert, F. Y. Kuhnert, K. Buse, J. R. Adleman, and D. Psaltis, "Trapping of dielectric particles with light-induced space-charge fields," *Appl. Phys. Lett.* **75**, 241909-241909-3 (2007).
- [10] X. Zhang, J. Wang, B. Tang, X. Tan, R. A. Rupp, L. Pan, Y. Kong, Q. Sun, and J. Xu, "Optical trapping and manipulation of metallic micro/nanoparticles via photorefractive crystals," *Opt. Express* **17**, 9981-9988 (2009).
- [11] M. Esseling, F. Holtmann, M. Woerdemann, and C. Denz, "Two-dimensional dielectrophoretic particle trapping in a hybrid crystal/PDMS-system," *Opt. Express* **18**, 17404-17411 (2010).
- [12] C. Arregui, J. B. Ramiro, Ángel Alcázar, Ángel Méndez, H. Burgos, Ángel García-Cabañes, and M. Carrascosa, "Optoelectronic tweezers under arbitrary illumination patterns: theoretical simulations and comparison to experiment," *Opt. Express* **22**, 29099-29110 (2014).
- [13] S. Glaesener, M. Esseling, and C. Denz, "Multiplexing and switching of virtual electrodes in optoelectronic tweezers based on lithium niobate," *Opt. Lett.* **37**, 3744-3746 (2012).
- [14] M. Esseling, A. Zaltron, N. Argiolas, G. Nava, J. Imbrock, I. Cristiani, C. Sada, et al. "Highly reduced iron-doped lithium niobate for optoelectronic tweezers," *Appl. Phys. B* **113** 191-197 (2013).
- [15] H. Burgos, M. Jubera, J. Villarroel, A. García-Cabañes, F. Agulló-López, and M. Carrascosa, "Role of particle anisotropy and deposition method on the patterning of nano-objects by the photovoltaic effect in LiNbO_3 ," *Opt. Mater.* **35**, 1700-1705 (2013).
- [16] M. Esseling, A. Zaltron, C. Sada, and C. Denz, "Charge sensor and particle trap based on Z-cut lithium niobate," *Appl. Phys. Lett.* **103**, 061115-061115-4 (2013).
- [17] M. Jubera, A. García-Cabañes, J. Olivares, A. Alcazar, and M. Carrascosa, "Particle trapping and structuring on the surface of $\text{LiNbO}_3\text{:Fe}$ optical waveguides using photovoltaic fields," *Opt. Lett.* **39** 649-652 (2014).
- [18] J. Matarrubia, A. García-Cabañes, J. L. Plaza, F. Agulló-López, and M. Carrascosa, "Optimization of particle trapping and patterning via photovoltaic tweezers: role of light modulation and particle size," *J. Phys. D Appl. Phys.* **47**, 265101 (2014).
- [19] N. V. Kukhtarev, V. B. Markov, S. G. Odulov, M. S. Soskin, and V. L. Vinetskii, "Holographic storage in electrooptic crystals-2. Beam coupling - light amplification," *Ferroelectrics* **22**, 961-964 (1979).
- [20] M. Carrascosa and F. Agulló-López, "Theoretical modeling of the fixing and developing of holographic gratings in LiNbO_3 ," *J. Opt. Soc. Am. B* **7**, 2317-2322 (1990).
- [21] L. Miccio, P. Memmolo, S. Grilli, and P. Ferraro, "All-optical microfluidic chips for reconfigurable dielectrophoretic trapping through SLM light induced patterning," *Lab. Chip.* **12**, 4449-4454 (2012).
- [22] F. Agulló-López, G. Calvo, and M. Carrascosa, "Fundamentals of Photorefractive Phenomena" in *Photorefractive Materials and Their Applications 1*, P. Günter and J.-P. Huignard, eds., 43-82 (Springer, New York, 2006).
- [23] H. A. Pohl, *Dielectrophoresis : the behavior of neutral matter in nonuniform electric fields* (Cambridge University Press Cambridge, New York, 1978).
- [24] J. Voldman, "Electrical forces for microscale cell manipulation," *Annu. Rev. Biomed. Eng.* **8**, 425-454 (2006).
- [25] P. Mokry, M. Marvan, and J. Fousek, "Patterning of dielectric nanoparticles using dielectrophoretic forces generated by ferroelectric polydomain films," *J. Appl. Phys.* **107**, 094104-094104-10 (2010).